

Molecular Order and Dynamics of Liquid-Crystal Side-Chain Polymers: An Electron Spin Resonance Study Employing Rigid Nitroxide Spin Probes

Karl-Heinz Wassmer,[†] Ernst Ohmes,[†] Michael Portugall,[‡] Helmut Ringsdorf,[‡] and Gerd Kothe^{*†}

Contribution from the Institute of Physical Chemistry, University of Stuttgart, D-7000 Stuttgart, Germany, and the Institute of Organic Chemistry, University of Mainz, D-6500 Mainz, Germany. Received May 21, 1984

Abstract: Rigid nitroxide radicals have proved to be sensitive and reliable spin probes of molecular order and dynamics in liquid-crystal side-chain polymers. Here we develop a comprehensive ESR line-shape model for these probes. The basis of our model is the stochastic Liouville equation, which we solve using a finite grid-point method. Particular emphasis is given to the slow-motional regime, characteristic of polymers in the liquid-crystal state. The theory is employed to the analysis of angular-dependent line shapes of cholestane spin probes, incorporated into macroscopically aligned polyacrylates with mesogenic side groups, differing in spacer length and molecular weight. Computer simulations provide the orientational distributions and rotational correlation times of the spin probes. They are related to molecular order and dynamics of the polymers **1a**, **1b**, **1c**, **2a**, **2b**, and their monomeric analogues **3** (see Figure 1). The rotational correlation times $\tau_{R\parallel}$ vary by four orders of magnitude ($0.2 \text{ ns} \leq \tau_{R\parallel} \leq 2000 \text{ ns}$). Logarithmic plots of $\tau_{R\parallel}$ vs. $1/T$ are linear within a phase, showing discontinuities at the phase transitions. Generally, $\tau_{R\parallel}$ in polymer **1b** (short spacer) is 300 times longer than $\tau_{R\parallel}$ in the monomeric analogue **3**, when referred to the same temperature in the nematic phase. This enormous slowdown of $\tau_{R\parallel}$ in the polymer indicates a strong dynamic coupling of main- and side-chain motions via the short spacer. As predicted, this dynamic coupling is weaker in the case of polymer **2b**, having the long spacer. From the rotational correlation times, intrinsic viscosities are determined. At $T = 385 \text{ K}$ the viscosities of **1b**, **2b**, and **3** are $\eta = 6.9 \times 10^{-1}$, 6.4×10^{-2} , and $1.9 \times 10^{-3} \text{ Ns/m}^2$, respectively, implying that the electrooptical response times of the liquid-crystal polymers are at least a factor of 30 longer than those of the corresponding monomers under the same conditions. The microorder of the various systems is discussed in terms of order parameters S_{ZZ} , characterizing the average orientation of the mesogenic units with respect to a local director. At the isotropic nematic transition, S_{ZZ} jumps to a finite value and then increases with decreasing temperature to $S_{ZZ} = 0.65$. Further jumps of S_{ZZ} , observed for the polymer **2a** and **2b**, indicate transitions to smectic A phases. Surprisingly, the observed order parameters are as high as those of the monomeric analogues. However, in contrast to conventional liquid crystals, long-range orientational order is retained in the solid state. Macroscopic alignment of the various systems is attempted with a variable magnetic field ($0.37 \leq B \leq 0.77$) and a constant electric field (50 kV/cm, 50 kHz). The degree of alignment achieved is described in terms of macroorder parameters, characterizing the orientation of the director axes in the sample system. Generally, complete alignment with respect to the electric field but only partial ordering by the magnetic field is observed. From the threshold fields, above which deformation of the macroorder occurs, the elastic constants of the liquid-crystal polymers are determined. For short spacers, these constants are at least one or two orders of magnitude larger than those of the monomeric analogues. In case of a sufficiently long spacer, however, the elastic constants are of the same magnitude. Interestingly, the macroorder of liquid-crystal polymers can be frozen in at the glass transition. No electric or magnetic field is required to maintain the director distribution in the sample. This particular property of liquid-crystal side-chain polymers opens new applications in the storage and display technology.

Introduction

Thermotropic liquid-crystal polymers with mesogenic side groups have attracted increasing current interest, both because of their theoretical and technological aspects.¹ The crucial point in a systematic preparation of such polymers was the introduction of flexible spacers, which separate the mesogenic units from the polymer backbone. Thus, a variety of liquid-crystal polymers has already been prepared.²⁻⁵ While considerable interest has centered around their synthetic design and macroscopic behavior, relatively little attention has focused on the dynamic and structural features

of the molecular units. Unknown so far are any details about molecular motion in the different polymer phases. Moreover, there is only limited information about the microorder of the mesogenic groups⁶⁻⁸ and the alignment of the domains in electric⁹ and magnetic fields.¹⁰

In the present study we investigate these properties with electron spin resonance (ESR) spectroscopy, employing nitroxide radicals as spin probes. They are widely used in liquid-crystalline systems, since their ESR spectra contain valuable information about the order and dynamics of the molecular environment. However, the

[†] University of Stuttgart.

[‡] University of Mainz.

(1) (a) Blumstein, A. "Liquid Crystalline Order in Polymers"; Academic Press: New York, 1978. (b) Ciferri, A.; Krigbaum, W. R.; Meyer, R. B., Eds. "Polymer Liquid Crystals"; Academic Press: New York, 1982.

(2) Finkelmann, H.; Ringsdorf, H.; Wendorff, J. H. *Makromol. Chem.* **1978**, *179*, 273-276. Finkelmann, H.; Happ, M.; Portugall, M.; Ringsdorf, H. *Ibid.* **1978**, *179*, 2541-2544. Finkelmann, H.; Koldehoff, J.; Ringsdorf, H. *Angew. Chem.* **1978**, *90*, 992-993. Ringsdorf, H.; Schneller, A. *Br. Polym. J.* **1981**, *13*, 43-46. Ringsdorf, H.; Schneller, A. *Makromol. Chem., Rapid Commun.* **1982**, *3*, 557-562.

(3) Shibaev, V. P.; Platé, N. A. *Polym. Sci. USSR* **1978**, *19*, 1065-1122. Shibaev, V. P.; Platé, N. A.; Freidzon, Y. S. *J. Polym. Sci., Polym. Chem. Ed.* **1979**, *17*, 1655-1670. Shibaev, V. P.; Talroze, F. I.; Karakhanova, F. I.; Platé, N. A. *Ibid.* **1979**, *17*, 1671-1684. Shibaev, V. P.; Kostromin, S. G.; Platé, N. A. *Br. Polym. J.* **1982**, *18*, 651-659.

(4) Finkelmann, H.; Rehage, G. *Makromol. Chem., Rapid Commun.* **1980**, *1*, 31-34. Finkelmann, H.; Rehage, G. *Ibid.* **1980**, *1*, 733-740. Finkelmann, H.; Kock, H.-J.; Rehage, G. *Ibid.* **1981**, *2*, 317-322. Finkelmann, H.; Rehage, G. *Ibid.* **1982**, *3*, 859-864.

(5) Portugall, M.; Ringsdorf, H.; Zentel, R. *Macromol. Chem.* **1982**, *183*, 2311-2321.

(6) Kothe, G.; Wassmer, K.-H.; Ohmes, E.; Portugall, M.; Ringsdorf, H. In "Liquid Crystals of One- and Two-Dimensional Order"; Springer Series in Chemical Physics 11; Helfrich, W.; Heppke, G., Eds.; Springer: Berlin, 1980; p 259. Wassmer, K.-H.; Ohmes, E.; Kothe, G.; Portugall, M.; Ringsdorf, H. *Makromol. Chem., Rapid Commun.* **1982**, *3*, 281-285.

(7) Geib, H.; Hisgen, B.; Pschorn, U.; Ringsdorf, H.; Spiess, H. W. *J. Am. Chem. Soc.* **1982**, *104*, 917-919. Boeffel, Ch.; Hisgen, B.; Pschorn, U.; Ringsdorf, H.; Spiess, H. W. *Isr. J. Chem.* **1983**, *23*, 388-394.

(8) Finkelmann, H. In ref 1b, pp 35-62. Finkelmann, H.; Benthack, H.; Rehage, G. *J. Chim. Phys.* **1983**, *80*, 163-171.

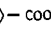

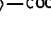

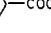


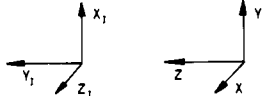
STRUCTURE	ACRONYM
$\text{-(CH}_2\text{-CH)}_x\text{-}$ COO-(CH ₂) ₂ -O-  -COO-  -OCH ₃	1a ($\bar{M}_n = 4500$) 1b ($\bar{M}_n = 14000$) 1c ($\bar{M}_n = 21000$)
$\text{-(CH}_2\text{-CH)}_x\text{-}$ COO-(CH ₂) ₆ -O-  -COO-  -OCH ₃	2a ($\bar{M}_n = 2500$) 2b ($\bar{M}_n = 14000$)
C ₁₀ H ₂₁ -O-  -COO-  -OC ₁₀ H ₂₁	3
 	CSL

Figure 1. Structures of the liquid-crystal systems studied and spin probes used in this work. Molecular coordinate systems of the nitroxide radical, diagonalizing the magnetic (X_1, Y_1, Z_1) and diffusion tensors (X, Y, Z), are also indicated.

difficulty of the method lies in proper analysis of the ESR spectra, the complexity being dependent on the relevant dynamic range. Unfortunately, spectral simulations in the slow-motional region, characteristic of polymers in the liquid-crystal state, require rather complex line-shape models as well as extensive amounts of computer time and memory.

In the first section we develop the theory necessary to understand the ESR spectra of nitroxide spin probes in liquid-crystal polymers. The basis of our model is the stochastic Liouville equation, which we solve, using a finite grid-point method. Particular emphasis is given to the slow-motional regime, where the conventional theories no longer apply. The line shapes are calculated from a spin Hamiltonian, which considers Zeeman and hyperfine interactions of nitroxide radicals, including pseudosecular contributions. No adiabatic approximation is used.

The theory is then applied to the analysis of temperature- and angular-dependent ESR spectra of rigid nitroxide spin probes, incorporated in macroscopically aligned polyacrylates with mesogenic side groups (Figure 1). For comparison, the low molecular weight analogues are also studied. Computer simulations provide the orientational distributions and rotational correlation times of the spin probes. They are related to molecular order and dynamics of the liquid-crystal polymers and their monomeric analogues.

From the rotational correlation times intrinsic dynamic properties of liquid-crystal polymers are determined. The orientational distributions of the spin probes sensitively reflect the microorder of the mesogenic units and its dependence on spacer length and molecular weight. Detailed information about the macroscopic alignment in electric and magnetic fields is obtained. The results, referring to all polymer phases including the glassy state, are discussed in relation to technological applications of these systems.

Theory

In this section we briefly develop an ESR line-shape model for nitroxide spin probes with particular reference to the slow-motional

(9) Finkelmann, H.; Naegle, D.; Ringsdorf, H. *Macromol. Chem.* **1979**, *180*, 803-806. Ringsdorf, H.; Schmidt, H.-W.; Schneller, A. *Macromol. Chem., Rapid Commun.* **1982**, *3*, 745-751. Ringsdorf, H.; Zentel, R. *Macromol. Chem.* **1982**, *183*, 1245-1256. Finkelmann, H.; Kiechle, U.; Rehage, G. *Mol. Cryst. Liq. Cryst.* **1983**, *94*, 343-358. Talroze, R. V.; Kostromin, S. G.; Shibaev, V. P.; Platé, N. A.; Kresse, H.; Sauer, K.; Demus, D. *Macromol. Chem., Rapid Commun.* **1981**, *2*, 305-309. Shibaev, V. P.; Platé, N. A. In "Liquid Crystal Polymers II/III"; Advances in Polymer Science 60/61; Gordon, M., Platé, N. A., Eds.; Springer: Berlin, 1984; pp 171-252.

(10) Archard, M. F.; Sigaud, G.; Hardouin, F.; Weill, C.; Finkelmann, H. *Mol. Cryst. Liq. Cryst. (Lett.)* **1983**, *92*, 111-118. Casagrande, C.; Veyssie, M.; Weill, C.; Finkelmann, H. *Ibid.* **1983**, *92*, 49-55. Fabre, P.; Casagrande, C.; Veyssie, M.; Finkelmann, H. *Phys. Rev. Lett.* **1984**, *53*, 993-996.

regime, where the conventional Redfield theory¹¹ no longer applies. Theories for such line shapes have been developed using an adiabatic assumption.¹² But this assumption often breaks down seriously in the case of hyperfine interactions in nitroxide radicals. A formally complete treatment, based on the stochastic Liouville equation, has been presented by Freed and co-workers, employing an eigenfunction expansion method.^{13a}

Here we develop an alternative model, using the stochastic Liouville approach. Molecular motion in our model is considered by a discrete Master equation, which we treat, using a finite grid-point method.^{13b} The line shapes are calculated for a comprehensive distribution function, in which director and magnetic field may have arbitrary orientations.

Generally, the absorption line shape $L(\omega)$ for an ensemble of radicals is given by

$$L(\omega) = \text{Im}\{\text{Tr}(\rho \cdot \mathbf{S}_+ \exp(-i\omega t))\} \quad (1)$$

where \mathbf{S}_+ is the raising operator, ω is the angular frequency of the microwave field, and ρ is the spin density matrix, assumed to obey the stochastic Liouville equation¹³⁻¹⁶

$$\begin{aligned} \dot{\rho}_{AB} &= (i/\hbar)[\rho_{AB}, \mathbf{H}_{AB}] + (\dot{\rho}_{AB})_{\text{relax}} + (\dot{\rho}_{AB})_{\text{rotidif}} \\ (\dot{\rho}_{AB})_{\text{rotidif}} &= \sum_{A'} (\mathbf{k}_{A'ABB} \rho_{A'B} - \mathbf{k}_{AA'B'} \rho_{AB}) + \\ &\quad \sum_{B'} (\mathbf{k}_{AAB'B'} \rho_{AB} - \mathbf{k}_{AABB'} \rho_{AB}) \end{aligned} \quad (2)$$

Here \mathbf{H}_{AB} is the spin Hamiltonian of the radical, $(\dot{\rho}_{AB})_{\text{relax}}$ is a phenomenological relaxation term, and $(\dot{\rho}_{AB})_{\text{rotidif}}$ accounts for the anisotropic rotational motion of the radicals. It is assumed that only a finite number of angular positions or sites, denoted by the index AB, can be occupied during this process. Each site is characterized by a set of Euler angles (θ_A, ϕ_B) relating the diffusion tensor system \mathbf{X}, \mathbf{Y} , and \mathbf{Z} to the laboratory system \mathbf{x}, \mathbf{y} , and \mathbf{z} , which we choose with the z axis parallel to the magnetic field (see Figure 2).

In the basis of the Zeeman functions $|M_s, M_l\rangle$

$$\begin{aligned} |1\rangle &= |\frac{1}{2}, 1\rangle & |2\rangle &= |\frac{1}{2}, 0\rangle & |3\rangle &= |\frac{1}{2}, -1\rangle \\ |4\rangle &= |-\frac{1}{2}, 1\rangle & |5\rangle &= |-\frac{1}{2}, 0\rangle & |6\rangle &= |-\frac{1}{2}, -1\rangle \end{aligned} \quad (3)$$

the matrices $\mathbf{k}_{AA'BB}$ in eq 2 are multiples of the unit matrix, characterizing the rate at which radicals at site AB move into site $A'B$. The values for the transition rates depend upon the model used to describe the motion. In the case of Brownian diffusion (reorientation through a sequence of infinitesimally small angular steps), the transition rates must satisfy the following equations:¹⁷

$$\begin{aligned} k_{AA+1BB} + k_{AA-1BB} &= N_A^2 / 3\pi^2 \tau_{R\perp} \\ k_{AABB+1} + k_{AABB-1} &= N_B^2 / 12\pi^2 \tau_{R\parallel} \\ k_{AA'BB''AB} &= k_{A'ABB''A'B} & k_{AABB''AB} &= k_{AAB''B''AB} \\ A, A' &= 1, 2, \dots, N_A & B, B' &= 1, 2, \dots, N_B \end{aligned} \quad (4)$$

where N_A, N_B are the number of orientations in θ and ϕ , respectively. Solving eq 4, one can establish values for all transition rates in terms of two rotational correlation times, $\tau_{R\perp}$ and $\tau_{R\parallel}$, and the equilibrium populations, n_{AB} , of the sites. $\tau_{R\perp}$ is the correlation time for reorientation of the symmetry axis of the

(11) Redfield, A. G. *Adv. Magn. Reson.* **1965**, *1*, 1-32.

(12) Itzkowitz, M. S. *J. Chem. Phys.* **1967**, *46*, 3048-3056. Korst, N. N.; Lazarev, A. V. *Mol. Phys.* **1969**, *17*, 481-487. Alexandrov, I. V.; Ivanova, A. N.; Korst, N. N.; Lazarev, A. V.; Prinkhozhenko, A. I.; Struykov, V. B. *Ibid.* **1970**, *18*, 681-691.

(13) (a) Freed, J. H.; Bruno, G. V.; Polnaszek, C. F. *J. Phys. Chem.* **1971**, *75*, 3385-3399. Polnaszek, C. F.; Bruno, G. V.; Freed, J. H. *J. Chem. Phys.* **1973**, *58*, 3185-3199. Polnaszek, C. F.; Freed, J. H. *J. Phys. Chem.* **1975**, *79*, 2283-2306. (b) Methods of solving the stochastic Liouville equation including nonsecular terms by means of finite differences have previously been employed in another context (see Freed, J. H.; Pedersen, J. B. *Adv. Magn. Reson.* **1976**, *8*, 1-84. Zientara, G. P.; Freed, J. H. *J. Phys. Chem.* **1979**, *83*, 3333-3345).

(14) Kubo, R. *Adv. Chem. Phys.* **1969**, *16*, 101-127.

(15) Norris, J. R.; Weissman, S. I. *J. Phys. Chem.* **1969**, *73*, 3119-3124.

(16) Kothe, G. *Mol. Phys.* **1977**, *33*, 147-158.

(17) Kothe, G.; Wassmer, K.-H.; Naujok, A.; Ohmes, E.; Rieser, J.; Wallenfels, K. *J. Magn. Reson.* **1979**, *36*, 425-434.

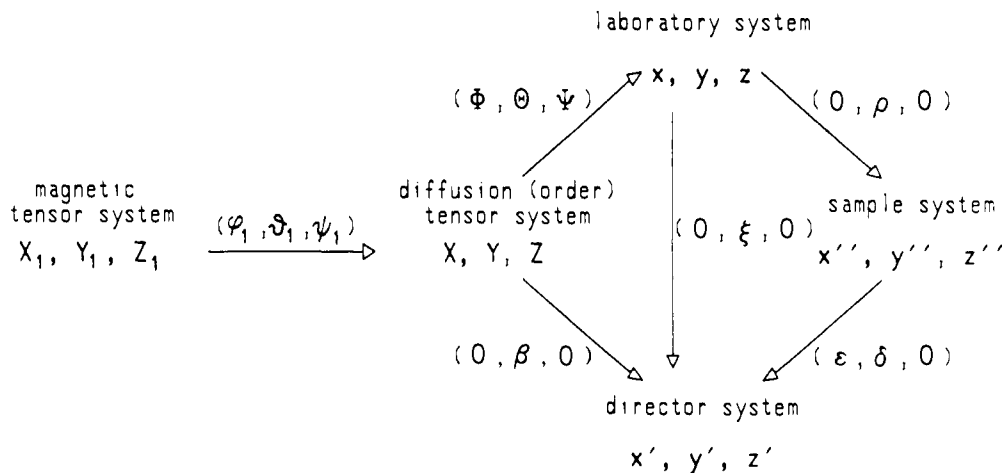


Figure 2. Notation for coordinate systems and Euler transformations used in the ESR line-shape model. The definition of the Euler angles corresponds to that of Van, Birrell, and Griffith.²⁰

diffusion tensor, while $\tau_{R\parallel}$ refers to rotation about it.

The population of a particular site is related to the normalized orientational distribution function

$$f(\phi, \theta, \Psi) = N_1 \exp[A(\cos \theta \cos \xi - \sin \theta \cos \Psi \sin \xi)^2] \quad (5)$$

by an integration over the area of that site. In deriving eq 5 from statistical theories of nematic liquid crystals,^{18a} we assumed that the order tensor is axially symmetric in X , Y , and Z . The coefficient A in eq 5 characterizes the orientation of the radicals with respect to a local director z' , while the angle ξ species the orientation of z' in the laboratory frame (Figure 2). In unaligned systems, the director axes are randomly distributed. In macroscopically ordered systems, however, z' can be specified with respect to a sample system x'' , y'' , and z'' , generally defined by the glass plate used to prepare the sample. If ρ denotes the angle between z'' (glass plate normal) and z , $\cos \xi$ is found to be

$$\cos \xi = \cos \delta \cos \rho - \sin \delta \cos \epsilon \sin \rho \quad (6)$$

where ϵ and δ are the polar coordinates of the director in the sample system (Figure 2). Of course, all director axes need not have the same orientation; instead they may be distributed according to the probability function

$$f(\epsilon, \delta) = N_2 \exp(B \cos^2 \delta + C \cos^2 \epsilon) \quad (7)$$

where the parameters B and C specify the orientation of the director axes in the sample system,^{18b} and N_2 is a normalization constant. The angles ϵ and δ are then varied, and each spectrum for a given set of angles is weighted by eq 7.

The spin Hamiltonian for a nitroxide radical may be written as

$$H_{AB} = \mu_B(g_{zz})_{AB}B_zS_z + (A_{xz})_{AB}S_zI_x + (A_{yz})_{AB}S_zI_y + (A_{zz})_{AB}S_zI_z + H_{n\text{-sec}} + H_{\text{rf}} \quad (8)$$

where

$$H_{\text{rf}} = g\mu_B B_1 S_x \exp(i\omega t) \quad (9)$$

and μ_B , $(g_{zz})_{AB}$, g , $(A_{xz})_{AB}$, B_z , B_1 , S , and I are the Bohr magneton, the zz component of the g tensor, and isotropic g factor, the xz component of the hyperfine tensor, the static magnetic field, the microwave field, the electron spin operator, and the ^{14}N nuclear spin operator, respectively. Since nonsecular terms $H_{n\text{-sec}}$ are only important at very rapid tumbling rates, which can be treated by the usual perturbation theory,^{11,19} we will ignore their effect.

(18) (a) Cotter, M. A. *J. Chem. Phys.* **1977**, *66*, 1098–1106. (b) The distribution function of eq 7 allows for biaxial ordering of the director axes, which may occur in simultaneously applied electric and magnetic fields.

(19) Freed, J. H.; Fraenkel, G. K. *J. Phys. Chem.* **1963**, *39*, 326–348. Nordio, P. L.; Rigatti, G.; Segre, U. *J. Chem. Phys.* **1972**, *56*, 2117–2123. Luckhurst, G. R.; Zannoni, C. *Proc. R. Soc. London, Ser. A* **1977**, *353*, 87–102.

The tensor elements in eq 8 are orientation dependent; consequently they fluctuate in time as the radical reorients. We can evaluate this orientation dependence by a twofold transformation from the magnetic system X_1 , Y_1 , Z_1 , which diagonalizes the g and hyperfine tensor. In the first step we transform to the diffusion tensor system X , Y , Z , using the Euler rotation matrix $T(\varphi_1, \theta_1, \psi_1)$:²⁰

$$A_{X,Y,Z} = T(\varphi_1, \theta_1, \psi_1) \cdot A_{X_1, Y_1, Z_1} \cdot T'(\varphi_1, \theta_1, \psi_1) \quad (10)$$

In the second step we rotate by the Euler angles $(\phi_B, \theta_A, 0)$ into the laboratory system x , y , z and obtain

$$(A_{x,y,z})_{AB} = T(\phi_B, \theta_A, 0) \cdot A_{X,Y,Z} \cdot T'(\phi_B, \theta_A, 0) \quad (11)$$

Evaluating the density matrix equation of motion (eq 2) in the basis of the Zeeman functions (eq 3) gives $36N_A N_B$ coupled differential equations

$$\begin{aligned} \rho_{ijAB} = & (i/\hbar) \sum_l (\rho_{ilAB} H_{ljAB} - H_{ilAB} \rho_{ljAB}) - \rho_{ijAB} [1/(T_2^0)_{ijAB} + \\ & k_{AA+1BB} + k_{AA-1BB} + k_{AABB+1} + k_{AABB-1}] + \rho_{ijA-1B} k_{A-1ABB} + \\ & \rho_{ijA+1B} k_{A+1ABB} + \rho_{ijAB-1} k_{AAB-1B} + \rho_{ijAB+1} k_{AAB+1B} + \\ & (i/\hbar) g\mu_B B_1 \exp(i\omega t) \cdot \sum_l [\rho_{ilAB} (S_x)_{lj} - (S_x)_{il} \rho_{ljAB}] \quad (12) \end{aligned}$$

$$i, j, l = 1, 2, \dots, 6$$

where $(1/T_2^0)_{ijAB}$ is a residual line width and the nonzero matrix elements are given by eq 13.

$$\begin{aligned} H_{11AB} &= (1/2)\mu_B(g_{zz})_{AB}B_z + (1/2)(A_{zz})_{AB} \\ H_{22AB} &= (1/2)\mu_B(g_{zz})_{AB}B_z \\ H_{33AB} &= (1/2)\mu_B(g_{zz})_{AB}B_z - (1/2)(A_{zz})_{AB} \\ H_{44AB} &= -H_{11AB}, H_{55AB} = -H_{22AB}, H_{66AB} = -H_{33AB} \\ H_{12AB} &= (\sqrt{2}/4)[(A_{xz})_{AB} - i(A_{yz})_{AB}] \\ H_{21AB} &= (\sqrt{2}/4)[(A_{xz})_{AB} + i(A_{yz})_{AB}] \\ H_{23AB} &= -H_{45AB} = -H_{56AB} = H_{12AB} \\ H_{32AB} &= -H_{54AB} = -H_{65AB} = H_{21AB} \\ (S_x)_{14} &= (S_x)_{25} = (S_x)_{36} = (S_x)_{41} = (S_x)_{52} = (S_x)_{63} = 1/2 \quad (13) \end{aligned}$$

For a weak microwave field we can take a steady-state solution of eq 12, and replace the density matrix elements of the last term by their thermal equilibrium values

$$\rho_{ijAB}^0 = \delta_{ij} n_{AB} \exp(-H_{ijAB}/kT) / \{\text{Tr}[\exp(-H_{ijAB}/kT)]\} \quad (14)$$

(20) Van, S. P.; Birrell, G. B.; Griffith, O. H. *J. Magn. Reson.* **1974**, *15*, 444–459.

Table I. Physical Properties of the Liquid-Crystal Systems Studied

liq cryst system ^a	spacer length ^b	mol wt ^c \bar{M}_n	phase transition temp, ^d T , K
1a	2	4 500	g 328 n 374 i
1b	2	14 000	g 335 n 388 i
1c	2	21 000	g 334 n 388 i
2a	6	2 500	g 296 s _A 361 n 381 i
2b	6	14 000	g 302 s _A 367 n 393 i
3			k 326 s _C 329 s _A 352 n 361 i

^a See Figure 1. ^b Number of segments. ^c Determined by vapor pressure osmometry. ^d Determined by polarization microscopy and DSC; k = crystalline, g = glassy, s_C = smectic C, s_A = smectic A, n = nematic, i = isotropic.

To proceed, we introduce

$$\rho_{ijAB} = \sigma_{ijAB} \exp(i\omega t) \quad (15)$$

and separate the exponential. In the steady state (slow passage)

$$\dot{\sigma}_{ijAB} = 0 \quad (16)$$

and four sets of $9N_A N_B$ coupled linear algebraic equations result. At high field the solution of only one set is required, which is readily accomplished by employing the Rutishauser²¹ or more efficiently the Lanczos algorithm.²² Summing up all contributions according to eq 1 finally gives the total line shape

$$L(\omega) = \text{Im}(\sqrt{2}\sigma_{41} + \sqrt{2}\sigma_{52} + \sqrt{2}\sigma_{63}) \quad (17)$$

In the following section the theory will be applied in the analysis of temperature and angular-dependent ESR spectra of nitroxide spin probes in oriented samples of liquid-crystal side-chain polymers.

Experiments and Methods

Materials. The liquid-crystal polymers poly[1-[2-[4-(4-methoxyphenoxy)phenoxy]ethoxy]ethyl] (1), poly[1-[6-[4-(4-methoxyphenoxy)phenoxy]hexyloxy]ethyl] (2), and the low molecular weight analogue *p*-*n*-decyloxybenzoic acid *p*'-*n*-butyloxyphenyl ester (3) were synthesized as described elsewhere^{5,23} (Figure 1). Average molecular weights of the polymers were determined by vapor pressure osmometry using CHCl₃ as solvent. The phase behavior of the liquid crystals was investigated by differential scanning calorimetry (DSC) (Perkin Elmer DSC-2C) and polarization microscopy (Leitz Ortholux II Pol BK). Table I lists relevant physical properties of the systems studied.

The spin probe 4',4'-dimethylspiro[5- α -cholestane-3,2'-oxazolidine]-3'-yloxy (CSL) was purchased from Syva and used without further purification. Figure 1 shows the structure of the nitroxide radical together with two molecular coordinate systems, which diagonalize the magnetic and rotational diffusion tensor, respectively.

Sample Preparation. Samples containing polymer 1 or 2 and a small amount of the spin probe (weight fraction < 10⁻³) were prepared from benzene solutions. The organic solvent was removed by freeze-drying overnight. Solutions of CSL in the low molecular weight liquid crystal 3 were prepared by proper mixing and heating. Addition of the spin probes depressed the transition temperatures of the systems by less than 1°. The doped liquid crystals were filled in special sample cells by heating them above the glass transition temperature or melting point, respectively.

The sample cell was constructed of two quartz plates, coated with tin dioxide to make them conducting.²⁴ The thickness of the cell, controlled by a Hostaphan spacer, was equal to 250 μ m. High-frequency electric fields (50 kHz) were employed to remove the influence of conductivity induced alignment of the director. The cell was placed in a home-built goniometer, attached to the microwave cavity, and the ESR spectrum was measured as a function of the angle ρ between quartz plate normal and magnetic field (Figure 2).

(21) Gordon, R. G.; Messenger, J. In "Electron Spin Relaxation in Liquids"; Muus, L. T., Atkins, P. W., Eds.; Plenum Press: New York, 1972; pp 341-381.

(22) Moro, G.; Freed, J. H. *J. Phys. Chem.* **1980**, *84*, 2837-2840. Moro, G.; Freed, J. H. *J. Chem. Phys.* **1981**, *74*, 3757-3773. Moro, G.; Freed, J. H. *Ibid.* **1981**, *75*, 3157-3159.

(23) Steinstraesser, R. *Z. Naturforsch.* **1972**, *276*, 774-779.

(24) Kothe, G.; Berthold, T.; Ohmes, E. *Mol. Phys.* **1980**, *40*, 1441-1451.

Macroscopic alignment of the samples was attempted shortly below the clearing temperature T_n with the quartz plate parallel to a magnetic field of 0.33 or 0.7 T. In addition, a high-frequency electric field of 50 kV/cm was applied. Saturation of the macroscopic alignment was checked by recording the ESR spectra as a function of time.

ESR Measurements. The ESR measurements were performed on a Varian E-9 X-band spectrometer, using 100-kHz field modulation. The spectrometer was interfaced with a Hewlett-Packard 9845 A computer, where the experimental spectra could be stored or transferred to a Univac 1100/80 computer. The scan range of the spectrometer was checked with an AEG nuclear magnetic resonance (NMR) gauss meter. The temperature of the sample was controlled by a home-built variable-temperature control unit and was stable to ± 0.2 K.

Spectral Analysis. The Fortran programs NOROTDIF and LANNOR were employed to analyze the experimental spectra. Both programs calculate ESR line shapes of nitroxide radicals undergoing fast, intermediate, and slow molecular reorientation in an anisotropic medium. LANNOR, based on the Lanczos algorithm,²² was found to yield accurate line shapes with at least order of magnitude reductions in computing time and computer storage requirements compared with the Rutishauser algorithm²¹ used in NOROTDIF. Typical running time for one spectrum of the nitroxide radical calculated with LANNOR on the Univac 1100/80 is 300 s ($N_A N_B = 120$).

Table II summarizes the constant parameters used in the calculations. They were obtained from a detailed analysis of rigid limit spectra. As observed previously, the hyperfine components slightly differ from system to system studied.²⁵ Note that the residual line widths include the effect of proton hyperfine interactions, omitted in the spin Hamiltonian. The orientation of the order and diffusion tensor is suggested by the geometry of the rigid radical (Figure 1). We assume that the order tensor is axially symmetric along **Z**. This assumption, tested by spectral simulations, reflects the overall shape of the radical, which is also expected to exhibit axially symmetric rotational diffusion about the **Z** axis. The orientation of the magnetic tensor relative to the diffusion tensor was determined from angular-dependent line shapes. The corresponding Euler angles φ_1 , θ_1 , ψ_1 (Figure 2) relating magnetic and diffusion tensor system are also listed in Table II. The values are in agreement with ESR studies of the CSL spin probe in single-crystals²⁶ except for a small tilt of the Y_1 axis relative to **Z**. However, the effect of this small tilt on the line shape is marginal.²⁵

The adjustable parameters $\tau_{R\parallel}$, $\tau_{R\perp}$, A , B , and C were determined by spectral simulations. In case of complete macroscopic alignment B and C need not be varied, and the remaining parameters were evaluated employing the following procedure. Each experimental spectrum at $\rho = 0$ and 90° is characterized by spectral parameters. From the separation and amplitudes of the lines in the $\rho = 0^\circ$ spectrum first estimates for $\tau_{R\parallel}$ and A are obtained. Independently, the $\rho = 90^\circ$ spectrum provides an estimate for the ratio $\tau_{R\perp}/\tau_{R\parallel}$. The values serve as start parameters in the complete simulation of a set of seven angular-dependent spectra at any given temperature. Having extracted the motions at some temperature points, their temperature dependence, usually a linear Arrhenius plot, is extrapolated into other regions. The reliability of this procedure has, of course, to be checked by comparing the simulated spectra with the corresponding experimental ones.

The analysis of spectra with incomplete macroscopic alignment is more involved. Generally, the parameters of micro- and macroorder affect the line shapes in different ways. However, reliable determination of A , B , and C requires independent variation. Since the macroorder is practically independent of temperature, B and C have to be determined only once for a given sample. The dynamic parameters $\tau_{R\parallel}$ and $\tau_{R\perp}$ and the microorder A can then be evaluated as described above.

Results

Macroscopically aligned samples of the liquid-crystal side-chain polymers 1a, 1b, 1c, 2a, 2b, and the low molecular weight analogue 3 were studied over a wide temperature range, using the CSL spin probes. Typical ESR spectra, varying drastically with temperature and sample orientation, are shown in Figures 3-5. They demonstrate the effect of the polymer chain, the spacer length, and the molecular weight on the spectral feature.

Figure 3 compares ESR spectra of the doped polymer 2b with those of the low molecular weight analogue 3. The spectra refer

(25) Rao, K.V.S.; Polnaszek, C. F.; Freed, J. H. *J. Phys. Chem.* **1977**, *81*, 449-456.

(26) Hubbell, W. L.; McConnell, H. M. *J. Am. Chem. Soc.* **1971**, *93*, 314-326. Marriott, T. B.; Birrell, G. B.; Griffith, O. H. *Ibid.* **1975**, *97*, 627-630.

Table II. Constant Parameters Used in the Calculation of the ESR Spectra of the CSL Spin Probes

	hyperfine tensor ^a in different systems, ^b mT			<i>g</i> tensor ^d	residual line width, ^c mT	magn tensor orientation, ^d deg
	1	2	3			
$A_{X_1X_1}$	0.60	0.58	0.59	$g_{X_1X_1}$, 2.008 8	$(1/T_2^0)_{41}$, 0.20	φ_1 , 270
$A_{Y_1Y_1}$	0.52	0.50	0.51	$g_{Y_1Y_1}$, 2.006 3	$(1/T_2^0)_{52}$, 0.21	ϑ_1 , 270
$A_{Z_1Z_1}$	3.35	3.31	3.29	$g_{Z_1Z_1}$, 2.002 2	$(1/T_2^0)_{63}$, 0.20	ψ_1 , 0

^a Diagonal in X_1, Y_1, Z_1 . ^b See Figure 1. ^c $(1/T_2^0)_{ij}$, independent of orientation, decrease with increasing temperature to limiting values of $(1/T_2^0)_{ij} = 0.18$ (1), 0.12 (2), and 0.055 mT (3), respectively. ^d Euler angles, relating magnetic and diffusion tensor system (Figure 2).

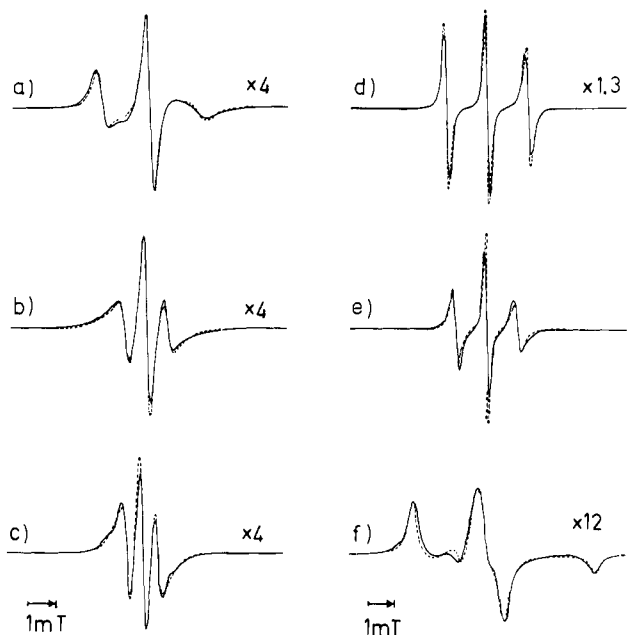


Figure 3. Experimental (—) and simulated (---) ESR spectra of the CSL spin probes in macroscopically aligned samples of the polymer **2b** (a–c) and the monomeric analogue **3** (d–f) at three different temperatures. The simulations were obtained with the parameters of Table II and refer to (a) $T = 393.5$ K, i, $\tau_{R\parallel} = 3$ ns, $\tau_{R\perp} = 21$ ns; (b) $T = 369$ K, n, $\tau_{R\parallel} = 7.8$ ns, $\tau_{R\perp} = 78$ ns, $S_{ZZ} = 0.63$, $S_{x'x'}$ = 1.0, $S_{z'z'}$ = -0.5; (c) $T = 263$ K, g, $\tau_{R\parallel}, \tau_{R\perp} > 2000$ ns, $S_{ZZ} = 0.92$, $S_{x'x'}$ = 1.0, $S_{z'z'}$ = -0.5; (d) $T = 370$ K, i, $\tau_{R\parallel} = 0.27$ ns, $\tau_{R\perp} = 1.35$ ns; (e) $T = 360$ K, n, $\tau_{R\parallel} = 0.4$ ns, $\tau_{R\perp} = 4$ ns, $S_{ZZ} = 0.48$, $S_{x'x'}$ = 1.0, $S_{z'z'}$ = -0.5; (f) $T = 263$ K, k, $\tau_{R\parallel}, \tau_{R\perp} > 2000$ ns, $S_{ZZ} = 0$. Note that all spectra refer to an angle $\rho = 90^\circ$ between quartz plate normal and magnetic field. i = isotropic, n = nematic, g = glassy, k = crystalline.

to a fixed orientation of quartz plate normal and magnetic field ($\rho = 90^\circ$) and three different temperatures, characterizing the isotropic, nematic, and solid state, respectively. The upper line shapes (Figure 3a,d), characteristic of an isotropic fluid medium, reflect distinct molecular motions in the two systems. Cooling below the clearing temperature causes drastic spectral changes. The central spectra (Figure 3b,e) now indicate oriented liquid-crystal phases. As one sees, molecular order is essentially retained when the polymer is cooled into the solid state (Figure 3c) in contrast with the low molecular weight liquid crystal exhibiting a random solid phase (Figure 3f).

Figure 4 compares the ESR spectra of the CSL spin probes in polymers **1b** and **2b**, demonstrating the effect of the spacer. The spectra refer to the same temperature ($T = 365$ K) but three different orientations ρ of glass plate normal and magnetic field. Drastic spectral changes are observed when the sample is rotated. Comparison of the spectra of **1b** (Figures 4a–c) and **2b** (Figures 4d–f) reveals the crucial effect of the spacer,^{2–5} affecting molecular order and dynamics, likewise. Note that both polymers have the same molecular structure and weight, differing in spacer length only.

In Figure 5 the effect of the molecular weight on the spectral feature is demonstrated. The ESR spectra refer to the solid polymers **1a** and **1b** ($T = 253$ K) and three different sample orientations. Interestingly, at $\rho = 0^\circ$ both polymers show identical

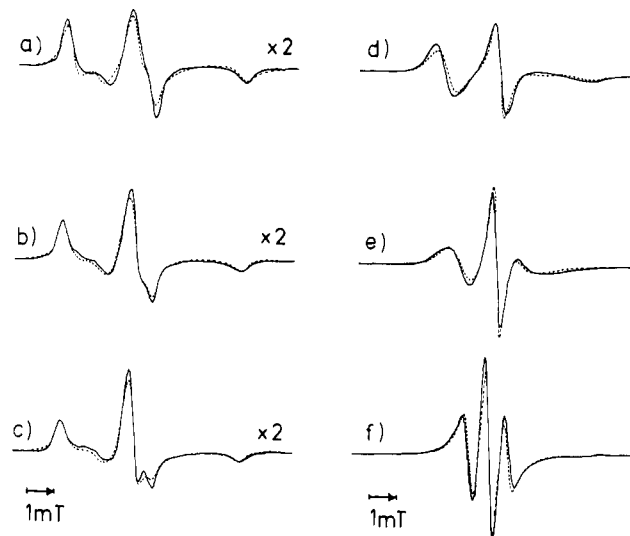


Figure 4. Experimental (—) and simulated (---) ESR spectra of the CSL spin probes in macroscopically aligned samples of the polymer **1b** (a–c) and **2b** (d–f) at $T = 365$ K and three different angles ρ between quartz plate normal and magnetic field. The simulations were obtained with the parameters of Table II and refer to (a) $\rho = 0^\circ$, $\tau_{R\parallel} = 86$ ns, $\tau_{R\perp} = 860$ ns, $S_{ZZ} = 0.62$, $S_{x'x'}$ = 0.2, $S_{z'z'}$ = -0.5; (b) $\rho = 50^\circ$; (c) $\rho = 90^\circ$; (d) $\rho = 0^\circ$, $\tau_{R\parallel} = 15$ ns, $\tau_{R\perp} = 150$ ns, $S_{ZZ} = 0.78$, $S_{x'x'}$ = 1.0, $S_{z'z'}$ = -0.5; (e) $\rho = 50^\circ$; (f) $\rho = 90^\circ$.

line shapes (Figure 5a,d). However, with increasing rotation angle significant differences appear, which are most pronounced in the $\rho = 90^\circ$ spectra (Figure 5c,f). Evidently, molecular order of liquid-crystal polymers also depends on the degree of polymerization.

Calculated spectra were fitted to the experimental spectra by applying the procedure outlined above. The dotted lines in Figures 3–5 represent best fit simulations. They agree favorably with their experimental counterparts. Figure 6 and 7 and Table IV summarize the parameters, obtained from the simulations, i.e., the rotational correlation times $\tau_{R\parallel}$ and $\tau_{R\perp}$ of the spin probes (see eq 4), the parameter of microorder A (see eq 5), and the parameters of macroorder B and C (see eq 7). In the following we would like to describe the results in more detail, treating the various simulation parameters separately.

Rotational Correlation Times. In Figure 6 the correlation times $\tau_{R\parallel}$ of the spin probes in the various systems are plotted as a function of $1/T$. They range from 0.2 to 2000 ns, implying that a fast-motional line-shape theory^{11,19} would be inadequate. Inspection of the logarithmic plots reveals several discontinuities, which occur at the phase-transition temperatures. Within a particular phase the plots are linear. From the slopes of the straight lines the rotational activation energies E_{rot} have been determined (Table III). As one can see, E_{rot} decreases with increasing order of the phase. Note the surprising low activation energies $15 \text{ kJ/mol} \leq E_{rot} \leq 25 \text{ kJ/mol}$ for the glassy state of the polymers. The anisotropy ratio $\tau_{R\perp}/\tau_{R\parallel}$ remains constant within a phase, varying from $\tau_{R\perp}/\tau_{R\parallel} = 5$ to $\tau_{R\perp}/\tau_{R\parallel} = 25$ (Table III). The uncertainty in correlation times is generally $<10\%$, except for $\tau_{R\parallel}, \tau_{R\perp} \geq 1000$ ns, where the effect on the line shape is marginal.

Microorder Parameters. The microorder of the spin probes is conveniently described in terms of the familiar order parameters

Table III. Dynamic Parameters Characterizing Different Phases of the Liquid-Crystal Systems Studied: Rotational Activation Energies E_{rot} (kJ/mol) and Anisotropy Ratio $\tau_{R\perp}/\tau_{R\parallel}$ in the Different Systems^a

phase ^b	1a		1b, 1c		2a		2b		3	
	E_{rot}	$\tau_{R\perp}/\tau_{R\parallel}$	E_{rot}	$\tau_{R\perp}/\tau_{R\parallel}$	E_{rot}	$\tau_{R\perp}/\tau_{R\parallel}$	E_{rot}	$\tau_{R\perp}/\tau_{R\parallel}$	E_{rot}	$\tau_{R\perp}/\tau_{R\parallel}$
i	83.6 ± 3.6	7	89.4 ± 3.6	7	74.9 ± 1.4	7	67.3 ± 3.4	7	53.8 ± 7.0	5
n	39.3 ± 0.9	10	45.4 ± 1.1	10	50.7 ± 4.6	10	58.1 ± 0.9	10	46.7 ± 6.3	10
s _A					45.8 ± 1.2	10	50.1 ± 0.8	10	25.9 ± 0.5	25
g	15.5 ± 0.4	10	15.2 ± 0.5	10	23.9 ± 1.0	10	24.9 ± 0.9	10		

^aSee Figure 1. ^bi = isotropic, n = nematic, s_A = smectic A, g = glassy.

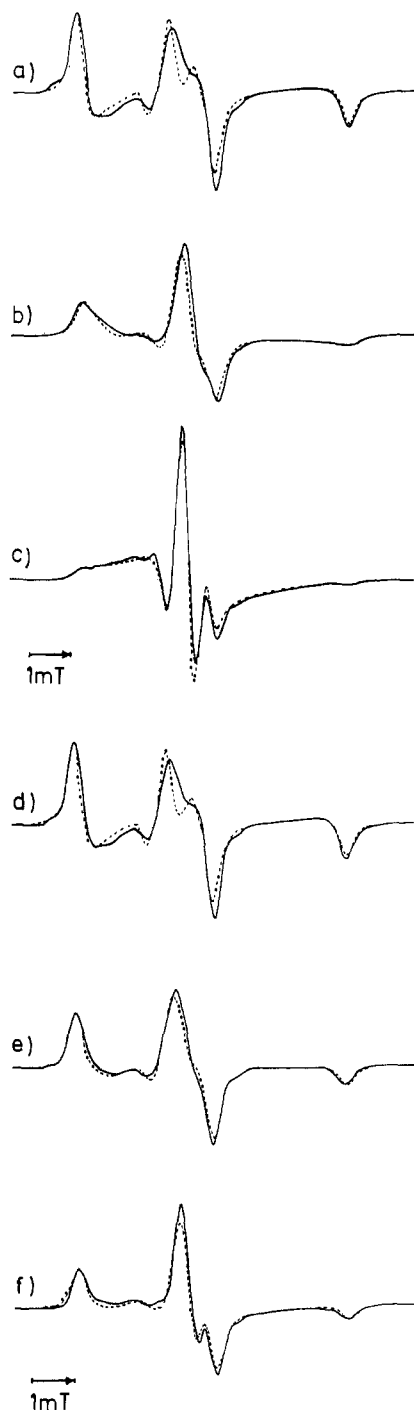


Figure 5. Experimental (—) and simulated (---) ESR spectra of the CSL spin probes in macroscopically aligned samples of the polymer **1a** (a-c) and **1b** (d-f) at $T = 253$ K and three different angles ρ between quartz plate normal and magnetic field. The simulations were obtained with the parameters of Table II and refer to (a) $\rho = 0^\circ$, $\tau_{R\parallel}, \tau_{R\perp} > 2000$ ns, $S_{ZZ} = 0.65$, $S_{x'x'} = 0.8$, $S_{z'z'} = -0.5$; (b) $\rho = 50^\circ$; (c) $\rho = 90^\circ$; (d) $\rho = 0^\circ$, $\tau_{R\parallel}, \tau_{R\perp} > 2000$ ns, $S_{ZZ} = 0.65$, $S_{x'x'} = 0.2$, $S_{z'z'} = -0.5$; (e) $\rho = 50^\circ$; (f) $\rho = 90^\circ$.

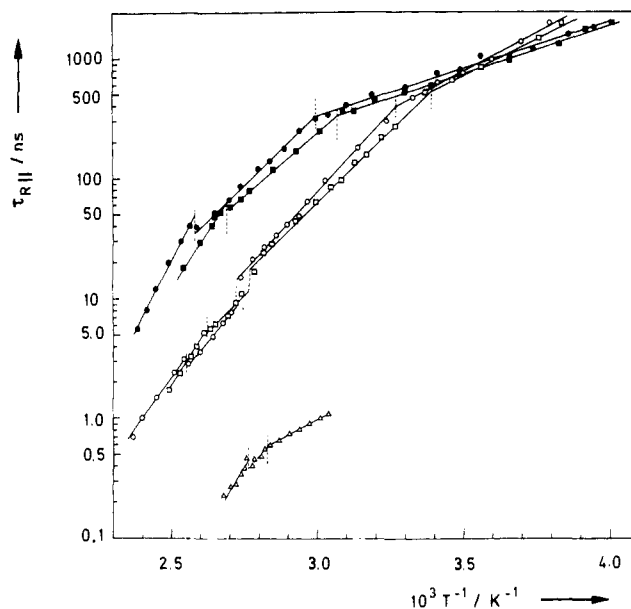


Figure 6. Arrhenius plot of the rotational correlation times τ_{Ri} of the CSL spin probes in various liquid-crystal systems. The correlation times refer to polymer **1a** (full squares), **1b** (full circles), **2a** (open squares), **2b** (open circles), and the low molecular weight analogue **3** (open triangles). Dotted lines indicate different phase transformations (see Table I).

S_{ZZ} , characterizing the average orientation of the molecular Z axis (see Figure 1) with respect to the director.²⁷ S_{ZZ} is readily calculated from the parameter A by evaluating the mean value integral:

$$S_{ZZ} = \frac{1}{2} N_1 \int_0^\pi (3 \cos^2 \beta - 1) \exp(A \cos^2 \beta) \sin \beta \, d\beta \quad (18)$$

In Figure 7 the order parameters S_{ZZ} of the spin probes in the various systems are plotted as a function of the reduced temperature $T^* = T/T_{ni}$. One sees that in the isotropic phase $S_{ZZ} = 0$. At the isotropic nematic transition ($T^* = 1.0$), the order parameters jump to finite values and then increase with decreasing temperature to $S_{ZZ} \approx 0.65$ in the nematic phases. Further jumps of S_{ZZ} , observed for the polymers **2a** and **2b**, indicate transitions to smectic A phases with limiting values of $S_{ZZ} \approx 0.92$. No such discontinuity is detected for the low molecular weight liquid crystal **3**. The maximum error for the microorder parameters is $\pm 3\%$.

Macroorder Parameters. The parameters B and C , characterizing the director distribution in the sample system, are conveniently discussed in terms of macroorder parameters $S_{x'x'}$, $S_{y'y'}$, and $S_{z'z'}$, defined by:^{27,28}

$$S_{x'x'} = \frac{1}{2} N_2 \int_0^\pi \int_0^{2\pi} (3 \sin^2 \delta \cos^2 \epsilon - 1) \exp(B \cos^2 \delta + C \cos^2 \epsilon) \sin \delta \, d\delta \, d\epsilon$$

$$S_{z'z'} = \frac{1}{2} N_2 \int_0^\pi \int_0^{2\pi} (3 \cos^2 \delta - 1) \exp(B \cos^2 \delta + C \cos^2 \epsilon) \sin \delta \, d\delta \, d\epsilon$$

$$S_{y'y'} = -(S_{x'x'} + S_{z'z'}) \quad (19)$$

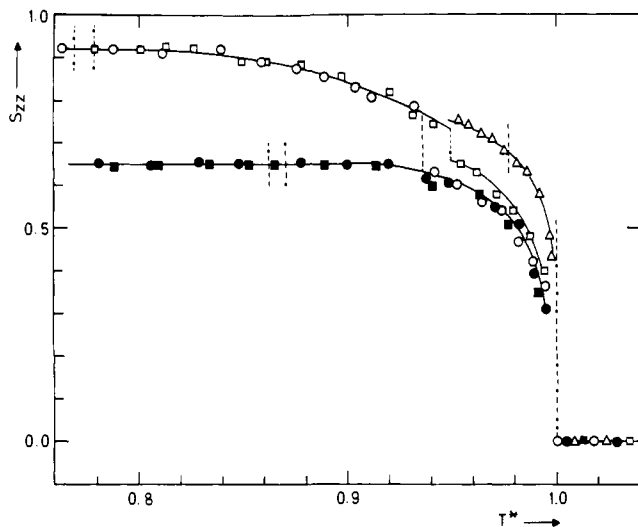


Figure 7. Temperature dependence of the microorder parameters S_{zz} of the CSL spin probes in various liquid-crystal systems. The order parameters refer to polymer **1a** (full squares), **1b** (full circles), **2a** (open squares), **2b** (open circles), and the low molecular weight analogue **3** (open triangles). Dotted lines indicate different phase transformations (see Table I). $T^* = T/T_{ni}$.

Values of these macroorder parameters, obtained for the various systems are listed in Table IV. One sees that $S_{z^{\prime}z^{\prime}}$ is always negative, exhibiting a limiting value of $S_{z^{\prime}z^{\prime}} = -0.5$, whereas $S_{x^{\prime}x^{\prime}}$ varies in the range $0.2 \leq S_{x^{\prime}x^{\prime}} \leq 1.0$. Of course, all these values refer to the special alignment conditions employed (see Table IV). The evolution of the macroscopic alignment in the liquid-crystal polymers is slow, even shortly below the clearing temperature. For instance, saturation of the macroscopic order of **2a** is reached in 600 s. Unequivocal determination of the macroorder parameters is always possible if the molecular motion is fast. The uncertainty in $S_{x^{\prime}x^{\prime}}$ and $S_{z^{\prime}z^{\prime}}$ depends on the degree of microorder and is generally $\leq 8\%$.

Discussion

The present knowledge about the molecular structure of liquid-crystal side-chain polymers originates to a great extent from X-ray diffraction studies.²⁹ While the packing of the mesogenic units in smectic phases has been well characterized, molecular organization in nematic and cholesteric phases is less clearly understood. Particularly, the arrangement of the polymer main chain, generally assumed to exhibit a random conformation, is still the subject of discussion.³⁰

Molecular order in liquid-crystal polymers is conveniently discussed in terms of micro- and macroorder parameters, characterizing the average orientation of the mesogenic units within a molecular domain and the macroscopic alignment of the domains. The measurement of these parameters is important for relating macroscopic physical properties of liquid-crystal polymers to their molecular structure. Various methods have been used to measure order parameters in these systems, including the use of birefringence and linear dichroism,⁸ but these methods can essentially not separate the two types of molecular order.³¹

(28) Mueller, K.; Wassmer, K.-H.; Lenz, R. W.; Kothe, G. *J. Polym. Sci., Polym. Lett. Ed.* **1983**, *21*, 785-789.

(29) Wendorff, J. H.; Finkelmann, H.; Ringsdorf, H. *J. Polym. Sci., Polym. Symp.* **1978**, *63*, 245-261. Wendorff, J. H. In "Liquid Crystalline Order in Polymers"; Blumstein, A., Ed.; Academic Press: New York, 1978; pp 1-41. Shibaev, V. P.; Moiseenko, V. M.; Freidzon, Y. S.; Platé, N. A. *Eur. Polym. J.* **1980**, *16*, 277-281. Magagnini, P. L. *Makromol. Chem., Suppl.* **4**, 1981, 223-240. Hahn, B.; Wendorff, J. H.; Portugall, M.; Ringsdorf, H. *Coll. Polym. Sci.* **1981**, *259*, 875-884. Kostromin, S. G.; Sinitzyn, V. V.; Talroze, R. V.; Shibaev, V. P.; Platé, N. A. *Makromol. Chem., Rapid Commun.* **1982**, *3*, 809-814. Tsukruk, V. T.; Shilov, V. V.; Lipatov, Y. S. *Makromol. Chem.* **1982**, *183*, 2009-2019. Tsukruk, V. V.; Lokhonya, O. A.; Shilov, V. V.; Kuzmina, V. A.; Lipatov, Y. S. *Makromol. Chem., Rapid Commun.* **1983**, *4*, 595-599.

Table IV. Parameters Characterizing the Macroscopic Alignment of the Liquid-Crystal Systems Studied

macroorder parameter ^a	alignment conditions ^b for the different systems ^c					
	1a		1b,c		2a,b	3
	0.33 T	0.70 T	0.33 T	0.70 T	0.33 T	0.33 T
$S_{x^{\prime}x^{\prime}}$	0.65	0.80	0.20	0.20	1.0	1.0
$S_{y^{\prime}y^{\prime}}$	-0.15	-0.30	0.30	0.30	-0.50	-0.50
$S_{z^{\prime}z^{\prime}}$	-0.50	-0.50	-0.50	-0.50	-0.50	-0.50

^a See eq 7 and 19. ^b Macroscopic alignment was attempted shortly below T_{ni} (see Table I) with the quartz plate of the electric field cell (50 kV/cm, 50 kHz) parallel to a magnetic field of 0.33 or 0.70 T (see Figure 2). ^c See Figure 1.

The magnetic resonance techniques employed such as ESR⁶ and ²H NMR⁷ do not suffer from this deficiency. ²H NMR has the principal advantage of detecting molecular order directly. However, analysis of the ²H NMR experiments requires knowledge of the molecular order tensor, not unambiguously defined because of conformational mobility. The use of rigid ESR probes offers the chance to determine the molecular order unequivocally.³² In addition, molecular dynamics of the different phases can be detected. In general, ESR spectra are sensitive to motions with correlation times between 10⁻¹⁰ and 10⁻⁶ s, a time range encountered for most motions in liquid-crystal polymers.

The rigid CSL probes used in this study have proved to be sensitive and reliable spin probes in thermotropic and lyotropic liquid crystals.³³⁻³⁶ They are thermally stable up to 450 K and exhibit an elongated rodlike shape with the order and rotational diffusion tensor parallel to the rod axis (see Figure 1). The preferential orientation and high ordering of the CSL probes in the liquid-crystal polymers indicates that they are located exclusively in the side-chain region. In the following, molecular order and dynamics will be discussed separately.

Molecular Dynamics. In Figure 6 the correlation times $\tau_{R\parallel}$ of the CSL spin probes in the various systems are plotted as a function of $1/T$. Similar plots are obtained for $\tau_{R\perp}$, employing the anisotropy ratios $\tau_{R\perp}/\tau_{R\parallel}$ listed in Table III. In the isotropic phases these ratios are consistent with the geometry of the probe ($\tau_{R\perp}/\tau_{R\parallel} = 4.7$). An apparent increase of $\tau_{R\perp}/\tau_{R\parallel}$, observed for the nematic and smectic phases, indicates anisotropic rotor-matrix interactions, as discussed by Freed and co-workers.³⁶ The correlation times $\tau_{R\parallel}$ of Figure 6, varying by four orders of magnitude, reflect the complex molecular dynamics of thermotropic side-chain polymers in the isotropic, liquid crystal, and glassy state.⁷ They refer to polymer **1a** (full squares), **1b** (full circles), **2a** (open squares), **2b** (open circles), and the low molecular weight analogue **3** (open triangles). Dotted lines indicate different phase transformations.³⁷ One sees that the plots are linear within a particular phase, showing discontinuities at the phase transitions. In passing from isotropic to nematic phases, small but distinct drops of $\tau_{R\parallel}$ are observed. In contrast, at the nematic smectic A transitions abrupt rises occur, in agreement with results on low molecular weight liquid crystals.^{36,38} Note the breaks at the glass transi-

(30) Zugenmaier, P.; Muegge, J. *Makromol. Chem., Rapid Commun.* **1984**, *5*, 11-19.

(31) Finkelmann, H.; Day, D. *Makromol. Chem.* **1979**, *180*, 2269-2274.

(32) Meier, P.; Blume, A.; Ohmes, E.; Neugebauer, F. A.; Kothe, G. *Biochemistry* **1982**, *21*, 526-534.

(33) Luckhurst, G. R.; Poupko, R. *Chem. Phys. Lett.* **1974**, *29*, 191-194. Luckhurst, G. R.; Setaka, M.; Zannoni, C. *Mol. Phys.* **1974**, *28*, 49-68. Luckhurst, G. R.; Yeates, R. N. *J. Chem. Soc., Faraday Trans. 2* **1976**, *72*, 996-1009.

(34) Meirovitch, E.; Luz, Z. *Mol. Phys.* **1975**, *30*, 1589-1602. Meirovitch, E.; Luz, Z.; Alexander, S. *Ibid.* **1979**, *37*, 1489-1507.

(35) Schreier, J.; Polnaszek, C. F.; Smith, I. C. P. *Biochim. Biophys. Acta* **1978**, *515*, 375-436.

(36) Meirovitch, E.; Freed, J. H. *J. Phys. Chem.* **1980**, *84*, 2459-2472. Meirovitch, E.; Freed, J. H. *Ibid.* **1980**, *84*, 3281-3295. Meirovitch, E.; Igner, D.; Igner, E.; Moro, G.; Freed, J. H. *J. Chem. Phys.* **1982**, *77*, 3915-3938.

(37) Frenzel, J.; Rehage, G. *Makromol. Chem., Rapid Commun.* **1980**, *1*, 129-134. Rehage, G.; Frenzel, J. *Br. Polym. J.* **1982**, *173*-179. Frenzel, J.; Rehage, G. *Makromol. Chem.* **1983**, *184*, 1685-1703.

(38) Lin, W.-J.; Freed, J. H. *J. Phys. Chem.* **1979**, *83*, 379-401.

tions,³⁹ indicating that the spin probes experience the motional state of the polymer backbone.

The rotational activation energies E_{rot} , evaluated from the Arrhenius plots, are listed in Table III. One sees that the highest values of 60 kJ/mol $< E_{\text{rot}} < 90$ kJ/mol refer to the isotropic phase. There is a systematic decrease in E_{rot} for all systems in the nematic and smectic A phase. The low values of 15 kJ/mol $< E_{\text{rot}} < 25$ kJ/mol, obtained for the glassy state of the polymers, indicate a change in the microscopic molecular dynamics.

The most striking feature of Figure 6 is the large difference in correlation times of polymers and low molecular weight analogues. Closer inspection reveals that $\tau_{R\parallel}$ in **1b** (full circles) is 300 times larger than $\tau_{R\parallel}$ in **3** (open triangles), when referred to the same temperature in the nematic phase. This enormous slowdown of $\tau_{R\parallel}$ in the polymer and the break of the Arrhenius plot at the glass transition indicate a strong coupling of main- and side-chain motions via the short spacer. As predicted,² this dynamic coupling is weaker in the case of polymer **2b** (open circles), having the long spacer. Note, however, that the correlation times in **2b** and **3** still differ by a factor of 30. Thus, decoupling of the mesogenic groups from the main chain, while effective, is not complete.

Comparison of the Arrhenius plots of **2a** (open squares) and **2b** (open circles) shows the effect of the molecular weight \bar{M}_n on the spin probe motion. Although \bar{M}_n increases from $\bar{M}_n = 2500$ to 14 000, $\tau_{R\parallel}$ is only slightly larger. Similar small effects are observed for polymer **1a** ($\bar{M}_n = 4500$, full squares), **1b** ($\bar{M}_n = 14 000$, full circles), and **1c** ($\bar{M}_n = 21 000$), which exhibits the same Arrhenius plot as **1b**. We therefore conclude that the molecular weight has an insignificant effect on the dynamics in the side-chain region.

The rotational correlation times $\tau_{R\parallel}$ of the CSL probes are related to the average viscosity η of the surrounding matrix by a modified Debye equation:

$$\tau_{R\parallel} = 4r_{\parallel}^3 \pi\eta / (3kT) \quad (20)$$

where r_{\parallel} is an effective rotation radius, depending upon the geometry of the probe and the nature of the rotor-matrix interactions. In favorable cases r_{\parallel} can be determined from ESR studies of the spin probe in a comparable matrix of known viscosity. A plot of $\tau_{R\parallel}$ vs. η/T for the CSL probes in nematic phase V^{40a} is linear over the whole temperature range investigated, yielding an effective rotation radius of $r_{\parallel} = 4.1 \times 10^{-10}$ m. We have taken this value to estimate the viscosities of the liquid-crystal polymers, not easily accessible otherwise.^{40b} In the nematic phase at $T = 385$ K the viscosities of **1b** and **2b** are $\eta = 6.9 \times 10^{-1}$ and 6.4×10^{-2} Ns/m², respectively. For comparison, the viscosity of the low molecular weight analogue **3** at the same temperature is $\eta = 1.9 \times 10^{-3}$ Ns/m².

These viscosities are of considerable interest for the use of liquid-crystal polymers in display and storage devices. It has been shown that the rise times t_R for electric and magnetic field induced deformations of the macroorder are given by⁴¹

$$t_R = \eta / [\Delta\epsilon\epsilon_0(E^2 - E_c^2)] \quad t_R = \eta / [\Delta\chi\mu_0(H^2 - H_c^2)] \quad (21)$$

where $\Delta\epsilon$, ϵ_0 , E , E_c , $\Delta\chi$, μ_0 , H , and H_c are the dielectric anisotropy of the system, the vacuum permittivity, the applied electric field strength, the threshold electric field, the diamagnetic anisotropy of the system, the vacuum permeability, the applied magnetic field strength, and the threshold magnetic field, respectively. One sees,

(39) Wasserman, A. M.; Alexandrova, T. A.; Buchachenko, A. L. *Eur. Polym. J.* **1976**, *12*, 691-695. Kovarskii, A. L.; Placek, J.; Szoecs, F. *Polymer* **1978**, *19*, 1137-1141. Weber, G.; Toernmaelae, P. *Colloid Polym. Sci.* **1978**, *256*, 638-644.

(40) (a) Steinstraesser, R.; Pohl, L. *Tetrahedron Lett.* **1971**, 1921-1923. The bulk viscosities η of nematic phase V were kindly provided by Dr. Pohl, Merck. (b) This procedure of determining viscosities presumes equal rotor-matrix interactions in the nematic phases of phase V and the liquid-crystal polymers.

(41) Leslie, F. M. *Arch. Ration. Mech. Anal.* **1968**, *28*, 265-283. Erickson, J. L. *Mol. Cryst. Liq. Cryst.* **1969**, *7*, 153-164. Parodi, O. *J. Phys. (Paris)* **1970**, *31*, 581-584.

that t_R is proportional to the viscosity, which crucially depends upon the spacer length. Thus, we expect the rise times of the liquid-crystal polymers to be at least a factor of 30 (long spacer) or 300 (short spacer) longer than those of the corresponding monomers under the same conditions. These predictions are in agreement with recent measurements of t_R in electric⁹ and magnetic fields.¹⁰

Microorder. In Figure 7 the microorder parameters S_{ZZ} of the CSL spin probes in the various systems are plotted as a function of the reduced temperatures $T^* = T/T_{ni}$. They refer to polymer **1a** (full squares), **1b** (full circles), **2a** (open squares), **2b** (open circles), and the low molecular weight analogue **3** (open triangles). Dotted lines indicate different phase transformations.³⁷ One sees that in the isotropic phase $S_{ZZ} = 0$, indicating a random orientation of the spin probes. At the isotropic-nematic transition the order parameters jump to a finite value and then increase with decreasing temperature to $S_{ZZ} \approx 0.65$.⁶ Note, that the order parameter curve of polymers **1a** and **1b** exhibits a horizontal slope at the glass transition. Further jumps of S_{ZZ} , observed for the polymers **2a** and **2b**, indicate transitions to smectic A phases with a limiting value of $S_{ZZ} \approx 0.9$. No such discontinuity is detected for the monomeric liquid crystal **3**, exhibiting a smectic A phase, likewise. Comparison of the order parameters of Figure 7 with those of ²H NMR⁷ and birefringence studies⁸ shows that the CSL probes reliably reflect the microorder of the mesogenic groups.

Surprisingly, the limiting value of the nematic order parameter of the polymers, independent of spacer length and molecular weight, is as high as that of the monomeric analogue. Linkage of the mesogenic units to the polymer backbone does apparently not restrict their orientational order, even in the case of a short spacer. It is evident, however, that in the low molecular weight system the order parameter exhibits a much stronger temperature dependence than in the polymeric one. This, of course, reflects the wider nematic range of the polymers, incidently increasing with molecular weight. Above a certain degree of polymerization, however, the nematic range remains constant (see, e.g., **1b** and **1c** in Table I), according to a plateau effect, observed for liquid-crystal side and main-chain polymers.^{8,42}

Inspection of Figure 7 reveals that the order parameter S_{ZZ} is quantitatively retained when the polymer is cooled below the glass transition temperature. No change in S_{ZZ} is observed over a period of 2 years, keeping the sample at room temperature. Thus, in contrast to conventional mesogens, crystallization in the solid state is prohibited and long-range orientational order preserved. This particular behavior of liquid crystal polymers opens new applications, as we shall see in the last section.

Macroorder. Macroscopic alignment of the liquid-crystal polymers and low molecular weight analogues was attempted shortly below the clearing temperature at $T^* = 0.98$ with the quartz plates of the electric field cell (50 kV/cm, 50 kHz) parallel to the magnetic field of 0.33 or 0.7 T. The degree of alignment achieved is discussed in terms of macroorder parameters $S_{x'x'}$, $S_{y'y'}$, and $S_{z'z'}$, defined in eq 19. For a random distribution of the director axes $S_{x'x'} = S_{y'y'} = S_{z'z'} = 0$. In case of a complete uniform alignment we expect $S_{x'x'} = 1.0$ and $S_{y'y'} = S_{z'z'} = -0.5$, assuming positive diamagnetic and negative dielectric anisotropy.

Experimental values of the macroorder parameters obtained for the various systems are listed in Table IV. Drastic variations are observed. A complete uniform alignment of the director axes is achieved for the polymers **2a** and **2b** (long spacer) and the monomeric analogue **3**. The observed macroorder parameters confirm the assumptions about the diamagnetic and dielectric anisotropy, namely, $\Delta\chi > 0$ and $\Delta\epsilon < 0$. For the polymers **1a**, **1b**, and **1c** (short spacer), the situation is more complicated. One sees that $S_{z'z'}$ still exhibits the limiting value of $S_{z'z'} = -0.5$, implying complete alignment with respect to the electric field. However, variation of $S_{x'x'}$ in the range $0.2 \leq S_{x'x'} \leq 0.8$ indicates only partial ordering by the magnetic field. Note that $S_{x'x'}$ critically depends on the molecular weight of the system. For the

(42) Blumstein, R. B.; Stickless, E. M.; Blumstein, A. *Mol. Cryst. Liq. Cryst. (Lett.)* **1982**, *82*, 205-213.

polymers **1b** ($\bar{M}_n = 14\,000$) and **1c** ($\bar{M}_n = 21\,000$), the macroorder parameters $S_{x'x'} = 0.2$, $S_{y'y'} = 0.3$, and $S_{z'z'} = -0.5$ reflect a two-dimensional random distribution of the director axes. No magnetic field induced alignment is observed in contrast with polymer **1a** ($\bar{M}_n = 4500$), where partial ordering occurs. Apparently, the degree of alignment increases with increasing field strength from $S_{x'x'} = 0.65$ to $S_{x'x'} = 0.80$.

It has been shown that the magnetic field induced deformations of the macroorder only occur above a threshold field strength⁴³

$$H_c = (\pi/d)[\bar{k}/(\Delta\chi\mu_0)]^{1/2} \quad (22)$$

where d and \bar{k} are the thickness of the sample cell and the effective elastic constant of the system, respectively. Our ESR studies yield threshold fields of $B_c = 0.3$ T for polymer **1a** and $B_c > 0.7$ T for polymer **1b** at a reduced temperature of $T^* = 0.98$. Assuming a value of $\Delta\chi = 1 \times 10^{-6}$ (SI) for the diamagnetic anisotropy of the polymers,¹⁰ we calculate elastic constants of $\bar{k} = 4.7 \times 10^{-10}$ and $> 2.6 \times 10^{-9}$ N. Depending on the molecular weight, these elastic constants are at least one or two orders of magnitude larger than those of the corresponding monomers.⁴⁴ In case of a sufficient long spacer (polymers **2a** and **2b**), however, the threshold fields, and therefore the elastic constants, are of the same magnitude, in agreement with recent studies in electric⁹ and magnetic fields.¹⁰

Interestingly, the macroorder of the liquid-crystal polymers can be frozen in at the glass transition. No electric or magnetic field is required to maintain the director distribution in the sample. Therefore, the liquid-crystal side-chain polymers can be used as storage material. The information, which is inserted in the nematic state by an electric field, can be stored permanently in the glassy state of the material. This exceptional property of liquid-crystal side-chain polymers has recently been applied in a new laser-addressed thermo-optic storage device.⁴⁵ Further applications in the display technology are currently being developed.⁴⁶

Conclusions

Dynamic ESR spectroscopy in combination with an appropriate line-shape model has provided detailed information about molecular order and dynamics of liquid-crystal side-chain polymers. Principal conclusions that emerge from this angular-dependent spin-probe study are the following:

(1) Decoupling of main- and side-chain motions via flexible spacers while effective is not complete. Thus, even in the case of long spacers the viscosities and electro-optical response times of liquid-crystal polymers are at least one order of magnitude larger than those of the low molecular weight analogues under the same conditions.

(2) The nematic order parameters of liquid-crystal polymers, independent of spacer length and molecular weight, exhibit the same limiting values as the monomeric analogues. However, in contrast to conventional liquid crystals, long-range orientational order is maintained in the solid state.

(3) The macroscopic alignment of liquid-crystal polymers in electric and magnetic fields sensitively depends on spacer length and molecular weight. Only for sufficient long spacers are the threshold fields and elastic constants comparable to those of conventional liquid crystals. In any case, however, the macroorder achieved can be frozen in at the glass transition.

In summary, liquid-crystal side-chain polymers, because of their exceptional molecular properties, present new evolving materials in the storage and display technology.

Acknowledgment. The numerical calculations were carried out on a Univac 1100 at the computer centers of the University of Freiburg and Stuttgart. Financial support of this work by the Deutsche Forschungsgemeinschaft and Fonds der Chemischen Industrie is gratefully acknowledged.

Registry No. 1, 79462-29-6; 2, 82200-54-2; 3, 94645-34-8; CSL, 18353-76-9.

(43) Saupe, A. *Z. Naturforsch., Teil A* **1960**, *15*, 815-822. Gruler, H.; Scheffer, T. J.; Meier, G. *Ibid.* **1972**, *27*, 966-976.

(44) The elastic constant $\bar{k} = 1.6 \times 10^{-11}$ N of the low molecular weight liquid crystal **3** is based on data for nematic phase 9a (Merck).

(45) Shibaev, V. P.; Kostromin, S. G.; Platé, N. A.; Ivanov, S. A.; Vetrov, V. Y.; Yakovlev, I. A. *Polym. Commun.* **1983**, *24*, 364-365.

(46) Simon, R.; Coles, H. J. *Mol. Cryst. Liq. Cryst. (Lett.)* **1984**, *102*, 43-48.